thermo

MDPI

Article

Evaluating the Combustion Behavior and Kinetics of Çayırhan Coal: A Comprehensive Thermogravimetric and Thermodynamic Study

Gülbanu Koyundereli Çilgi * and Elif Çavdar

Department of Metallurgical and Materials Engineering, Faculty of Engineering and Natural Sciences, Manisa Celal Bayar University, 45140 Manisa, Turkey; elifardic97@gmail.com

* Correspondence: gulbanu.cilgi@cbu.edu.tr; Tel.: +90-236-2012418

Abstract

In this study, the combustion behavior of Çayırhan coal under an oxygen atmosphere was investigated, and its combustion kinetics and thermodynamic parameters were determined. Thermal analyses (TGA, DTG, and DSC) revealed that the combustion process occurs in two consecutive steps. The first step, in which 85% of the total weight loss takes place, requires a relatively low activation energy. Conversely, the second step, corresponding to the remaining 15% of the combustion, requires a significantly higher activation energy. Both combustion steps were analyzed using model-free isoconversional methods. The average activation energies were calculated as 139.65 ± 9.66 kJ/mol for Combustion 1 and 402.27 ± 65.53 kJ/mol for Combustion 2. Subsequent kinetic modeling studies demonstrated that both combustion reactions are highly compatible with the diffusion mechanism. Following the determination of the most suitable reaction model, the Arrhenius pre-exponential factor (A) and other thermodynamic parameters of the activated complex ($\Delta S^{\ddagger}$, $\Delta H^{\ddagger}$, and $\Delta G^{\ddagger}$) were successfully evaluated. These thermodynamic and kinetic insights clarify the distinct combustion regimes of Çayırhan coal under laboratory conditions. Ultimately, the selected diffusion-based kinetic models offer a practical baseline framework for evaluating combustion performance and providing preliminary insights for reactor considerations in low-rank coal applications.

Keywords: combustion behavior; Çayırhan coal; isoconversional methods; modeling methods; thermal analysis; thermodynamic parameters

1. Introduction

Energy, a fundamental input for social and economic development, is an indispensable component of modern life. Despite recent advancements in renewable energy technologies, fossil fuels maintain a dominant share within the global energy mix. Among these, coal, oil, and natural gas are hydrocarbon-based fossil fuels characterized by high carbon content. Due to limited domestic oil and natural gas reserves in Turkiye, along with the technical difficulties associated with large-scale natural gas storage, coal is of paramount importance for the country's energy strategy. For instance, as of late October 2024, coal-fired power plants constituted 19.1% of Turkiye's total installed power capacity [1]. Consequently, integrating domestic coal resources into the national economy is critical for ensuring energy security. However, the majority of Turkish coal reserves exhibit low carbon, high moisture, and high ash content [2,3]. To maximize the energy potential of these domestic resources, it

Check for updates

Received: 24 July 2026
Revised: 20 August 2026
Accepted: 7 September 2026
Published: 9 September 2026

Copyright: © 2026 by the authors. Licensee MDPI, Basel, Switzerland. This article is an open access article distributed under the terms and conditions of the Creative Commons Attribution (CC BY) license.

is crucial to implement physical and chemical pre-treatments, determine their precise combustion behaviors, mitigate spontaneous combustion risks, and comprehensively evaluate the parameters influencing combustion reactivity.

Thermal analysis techniques, such as Thermogravimetric Analysis (TGA), Differential Thermogravimetry (DTG), and Differential Scanning Calorimetry (DSC), are indispensable tools for investigating the combustion and pyrolysis reactions of coals [4–6]. TGA measures mass changes as a function of temperature, whereas DTG monitors the rate of mass changes. In the DTG method, these mass changes are resolved as distinct peaks, which significantly enhances the accuracy of determining reaction initiation and termination temperatures. On the other hand, DSC evaluates the amount of heat absorbed or released during a reaction, where the resulting peak areas are directly proportional to the enthalpy change. These integrated techniques are widely utilized to study the kinetics and thermodynamics of coal combustion and pyrolysis. For instance, Zhang et al. investigated the thermal properties of three coal types with varying degrees of coalification, determining their ignition points and spontaneous combustion temperatures and subsequently calculating combustion activation energies using the FWO and KAS methods [5]. Similarly, Dwivedi et al. examined the pyrolysis of low-rank and bituminous coals in a nitrogen atmosphere using TGA-DTG, employing the Friedman differential method for kinetic analysis. They reported that the pyrolysis activation energy varied over a wide range (34.66–396.52 kJ/mol) for the bituminous coal, whereas it remained within a narrow range (57.80–64.28 kJ/mol) for the low-rank coal [7]. Additionally, Wang et al. investigated the pyrolysis of Chinese bituminous coal using TGA data obtained at multiple heating rates. Applying the Doyle integral method, they established that the pyrolysis process conforms to a first-order reaction model and successfully calculated the corresponding thermodynamic parameters [4]. Furthermore, the pyrolysis of four low-to-medium-rank coals under a helium atmosphere was studied by Yan et al., who utilized the FWO, KAS, Starink, and Friedman isoconversional methods to evaluate kinetic and thermodynamic profiles, plotting the variation of activation energy and thermodynamic quantities against the conversion fraction [8]. Finally, Fan et al. analyzed the combustion kinetics of pre-oxidized coals under various oxygen concentrations using the FWO and KAS methods [9].

This study focuses on coal from the Çayırhan region of Türkiye to systematically examine its combustion behavior. Although some research exists on this specific reserve, detailed thermal analysis and combustion kinetics studies remain highly limited in the literature. For instance, Kök et al. investigated the combustion behavior of Çayırhan coal using the Friedman differential method [10]. However, instead of calculating the activation energies at progressive conversion fractions (α) throughout the combustion process, they evaluated the reaction stage as a whole, reporting only a single, overall activation energy. In addition, their work lacked any thermodynamic evaluation of the process.

To address such limitations in consecutive or multi-stage thermal degradation processes, conducting a detailed kinetic analysis is essential to establish the initiation and termination boundaries precisely for each individual reaction stage. For this purpose, a novel kinetic approach based on monitoring activation energy fluctuations across the entire process to clearly differentiate successive stages was previously proposed by our research group for the first time in the literature during our studies on uranium salts [11–13]. Evaluating the feasibility of this robust methodology on complex fuel matrices could offer a more precise understanding of coal combustion kinetics.

To the best of our knowledge, beyond this highly limited literature, no detailed study has been conducted on the comprehensive thermal, kinetic, and thermodynamic behavior of Çayırhan coal. To address this gap, proximate, elemental, and calorimetric analyses were initially performed to characterize the physical and chemical properties of the coal.

Subsequently, thermal analyses were carried out under a dynamic oxygen atmosphere (100 mL/min. flowing rate) utilizing simultaneous TGA-DTG-DSC techniques. Based on these experimental data, combustion kinetic parameters and thermodynamic quantities were rigorously calculated. In the kinetic evaluations, the model-free isoconversional methods of KAS and FWO were applied, while Composite Method 1 (CM I) and Composite Method 2 (CM-II) were employed for the thermodynamic assessments after identifying the governing reaction model. Through this multi-method framework, the present study indicates that diffusion-based models (D_3 for Combustion 1 and D_2 for Combustion 2) provide the best description of the kinetic reaction rate across progressive conversion fractions. Ultimately, these conversion-dependent kinetic and thermodynamic insights provide a practical baseline reference for evaluating thermal degradation behavior and offering initial considerations for low-rank coal applications.

2. Materials and Methods

2.1. Experimental Section

Coal samples were collected from the Çayırhan region of Türkiye. These samples were first crushed using a jaw crusher (Rantek, Ankara, Türkiye) and subsequently homogenized. To remove moisture, a 100 g portion of the coal sample was dried in an oven at 105 °C for approximately 4 h until a constant weight was achieved. The moisture-free coal samples were pulverized to a fine powder below 250 μm using a Rantek ring grinder to prepare them for subsequent analyses. This prepared stock coal was subsequently utilized for all further measurements. Proximate analysis was conducted using a LECO TGA801 thermogravimetric analyzer (LECO Corporation, St. Joseph, MI, USA), while ultimate analysis was performed using a LECO CHN-628 elemental analyzer, in accordance with ASTM D-5373 standards [14].

Additionally, the gross calorific value of the coal was determined using a LECO AC600 bomb calorimeter (LECO Corporation). The combustion process in this device was carried out using oxygen gas with a purity of 99.5%. The oxygen was supplied to the bomb at an average pressure of 31 bar, facilitated by an integrated oxygen filling and discharge station. Pure water with a pH of 6–8 was maintained at a constant temperature (around 15 °C) and was utilized for heat transfer between the inner and outer jackets. A sample of approximately 1 g was weighed and placed into the combustion crucible. Following the analysis, which lasted an average of 6 min, the gross calorific value (GCV) was obtained. The net calorific value (NCV) is subsequently calculated from this gross calorific value by accounting for the latent heat of vaporization of all water content; reporting the net calorific value is considered more appropriate for practical applications. The calculated net calorific value for our coal sample was determined as 9899.34 ± 120.25 J/g.

TGA, DTG and DSC analyses were realized with a TA Instruments SDT 650 apparatus (TA Instruments, New Castle, DE, USA). Prior to the thermal measurements, both temperature and mass calibrations of the simultaneous analyzer were meticulously performed. For the temperature calibration, high-purity indium (In) and tin (Sn) reference materials, provided by the manufacturer, were utilized. The temperature calibration was verified by measuring the melting points of these standards, yielding 156.6 ± 0.3 °C for In and 231.9 ± 0.4 °C for Sn, both of which are in excellent agreement with the certified values. For the mass calibration, certified standard weights supplied by the manufacturer were employed. The weight of a certified 20.05 mg standard was re-measured by the instrument, resulting in an average value of 20.04 ± 0.01 mg. Each calibration measurement was performed in triplicate, and the actual experimental runs were initiated only after ensuring the high precision and accuracy of these calibration steps.

Following the successful completion and verification of all calibration procedures, the experimental analysis of the coal samples was conducted under carefully optimized conditions. Mass transfer limitations are among the most common issues encountered in thermal measurements. To mitigate these effects, a small sample amount (approximately 10 mg) was utilized and spread evenly as a single, thin layer at the bottom of an alumina crucible. The thermal runs were performed from room temperature to 850 °C. To satisfy the requirements of the kinetic evaluations, the heating rates were varied at 5, 10, and 15 °C/min. An oxygen atmosphere was selected to facilitate the combustion reactions, with a constant dynamic flow rate maintained at 100 mL/min. These selected heating rates and the gas flow rate represent well-established, optimized parameters widely accepted in the literature for obtaining reliable kinetic data from coal combustion and pyrolysis [5,7,15]. Furthermore, consistent with these standard practices, a separate protective gas was not required, as the dynamic oxygen flow adequately functioned as the sole reaction and purge atmosphere during the runs.

2.2. Calculation Section

At the beginning of the study, combustion activation energy values were calculated using the KAS [16,17] and FWO [18,19] methods, which are integral-isoconversional methods widely used in the academic literature. These methods are also known as model-free methods because they calculate activation energy without assuming a specific reaction model equation for the overall mechanism. Instead, they rely on the isoconversional principle, which assumes that at a specific, constant conversion fraction (α), the reaction rate is a function solely of temperature, meaning that the reaction model function $g(\alpha)$ remains constant across different heating rates (β) for any given α. The final equations of these methods are stated below.

KAS equation:

$$\ln\left(\frac{\beta}{T^2}\right) = ln\left[\left(\frac{AR}{g(\alpha)E_\alpha}\right).\left(1-\frac{2RT}{E_\alpha}\right)\right] - \frac{E_\alpha}{R}\frac{1}{T} \quad (1)$$

FWO equation:

$$\ln\beta = -5.3305 + \ln\left(\frac{AE_\alpha}{g(\alpha)R}\right) - 1.052\frac{E_\alpha}{R}\frac{1}{T} \quad (2)$$

α is known as the reaction (combustion) ratio and is calculated using this formula: $\alpha = (w_i - w_t)/\left(w_i - w_f\right)$ where w_i, w_t, and w_f, are the initial weight of the sample, the weight of the sample at the examined time t, and the final weight of the sample at the end of the process, respectively. A stands for the pre-exponential factor. E_α is the activation energy corresponding to the combustion ratio, $g(\alpha)$ is an unknown function of the combustion, T indicates temperature in Kelvin, and R is the gas constant (8.314 J/mol.K).

In these methods, the plots of $\ln(\beta/T^2)$ versus $1/T$ (for KAS equation) and $\ln\beta$ versus $1/T$ for FWO equation) graphs are prepared for each α constant, and activation energy values are calculated by using these slope data.

To determine the reaction model, the KAS and FWO method equations are modified. Following this modification, the equations known in the academic literature as Composite Method I (CM I) [20] and Composite Method II (CM II) [21,22], given below, are obtained.

CM I equation:

$$\ln\left(\frac{g(\alpha)}{T^2}\right) = \ln\left[\left(\frac{AR}{\beta E_\alpha}\right).\left(1-\frac{2RT}{E_\alpha}\right)\right] - \frac{E_\alpha}{R}\frac{1}{T} \quad (3)$$

CM II equation:

$$\ln g(\alpha) = \ln\left(\frac{AE_\alpha}{\beta R}\right) - 5.3305 - 1.052\frac{E_\alpha}{R}\frac{1}{T} \quad (4)$$

In these methods, the process is performed for all conversion fractions in which the reaction occurs at a single β heating rate. Thus, the reaction is examined as a whole, not in parts. The advantage of these methods is that there is no requirement to work with different heating rates and, at the same time, the dominant pattern in the reaction is determined. For the relevant heating rate, the temperature T values are determined from the thermogram for all α conversion fractions, and the $g(\alpha)$ function values are calculated. $g(\alpha)$ functions describe the reaction model. Thirteen different $g(\alpha)$ functions are known in the literature [23,24]. These functions depend on nucleation, reaction-order-controlled, phase-boundary-controlled, and diffusion-controlled mechanisms. For each α value at a single heating rate (β), the values of $\ln[g(\alpha)/T^2]$ (for CM I) or $\ln[g(\alpha)]$ (for CM II) were calculated and plotted versus *1000/T* values. Similar calculations were repeated for thirteen different $g(\alpha)$ functions, and corresponding plots were drawn. The most suitable kinetic model was selected, which showed the lowest standard deviation, and the activation energies obtained from the CM I and CM II methods were compatible with those obtained from isoconversional procedures of the KAS and FWO methods with the best regression analysis (r^2) value.

The activated complex (transition state) theory is used for the calculation of $\Delta S^\ddagger$, $\Delta H^\ddagger$ and $\Delta G^\ddagger$. Related equations are given as below.

$$A = \left(\frac{k.T_{avg}}{h}\right)e^{(\Delta S^\ddagger/R)} \quad (5)$$

$$\Delta H^\ddagger = E_\alpha - RT_{avg} \quad (6)$$

$$\Delta G^\ddagger = \Delta H^\ddagger - T_{avg}\Delta S^\ddagger \quad (7)$$

where k is the Boltzmann constant (1.381×10^{-23} J/K), h denotes Planck's constant (6.626×10^{-34} J.s), T_{avg} corresponds to the average reaction temperature, and E_a stands for the activation energy, which was calculated from the slope of Composite Methods graphs for the selected model.

3. Results and Discussions

3.1. Physical Properties of Çayırhan Coal

Proximate and ultimate analyses were performed in triplicate, as described in the experimental section, and the average results are presented along with their corresponding standard deviations in Table 1. The obtained values indicate that the Çayırhan coal is characterized by a high volatile matter content and low fixed carbon. On one hand, volatile matter facilitates earlier ignition by lowering the coal's ignition temperature; on the other hand, it reduces the overall calorific value. Consequently, a high volatile matter content is undesirable as it acts as a key parameter that impairs combustion reactivity.

Table 1. Proximate and Ultimate Analyses of Çayırhan Coal (wt.% air-dry basis).

Proximate Analysis, air-dry basis %			
Moisture	Ash	Volatile Matter	Fixed C
0.81 ± 0.05	41.90 ± 0.10	40.70 ± 0.26	17.40 ± 0.18
Ultimate Analysis, air-dry basis %			
C	H	N	S
34.99 ± 0.06	3.27 ± 0.01	1.52 ± 0.08	1.45 ± 0.07

3.2. Thermal Analysis of Çayırhan Coal

In the literature, the thermal degradation of coals is widely reported to proceed through three primary stages: dehydration, combustion or pyrolysis, and mineral matter decomposition [2,4,25]. The initial dehydration stage is typically completed at temperatures up to approximately 150 °C. The subsequent stage, referred to as either pyrolysis or combustion, depends strictly on the carrier atmosphere employed; it is classified as pyrolysis under an inert atmosphere and as combustion when an oxygen or air atmosphere is utilized. During the final mineral decomposition stage, gas evolution occurs due to the breakdown of inorganic mineral matter natively present within the coal structure, such as clays, calcium carbonate, and magnesium carbonate [2,4,25]. Consistent with these literature trends, the TGA, DTG, and DSC curves of our sample, presented in Figure 1, clearly exhibit a similar three-stage degradation profile. However, distinct from most typical coals, the combustion stage of Çayırhan coal takes place in two consecutive steps. The first stage represents a rapid combustion phase in which approximately 85% of the total combustion is completed. The second stage, by contrast, is a relatively slower process wherein the remaining 15% of the combustion phase is fulfilled.

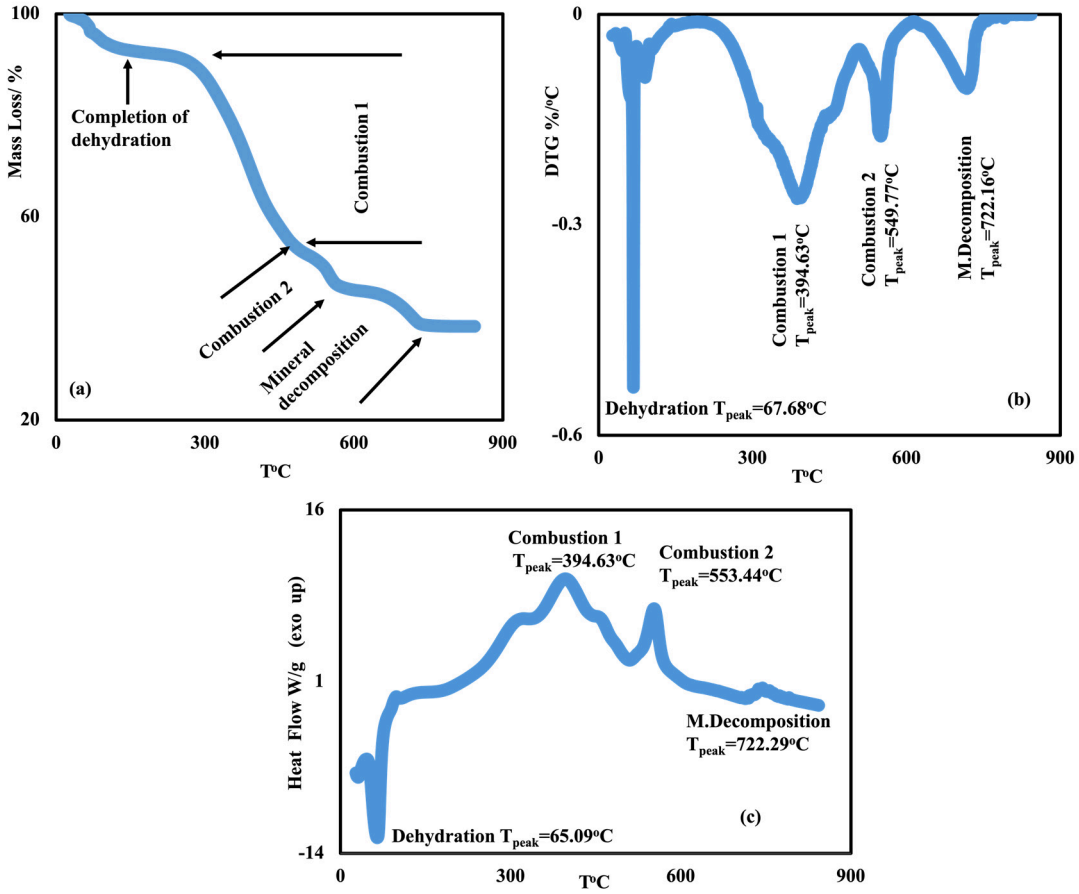


Figure 1. TGA (**a**), DTG (**b**) and DSC (**c**) curves of Çayırhan coal taken with a heating rate of 10 °C/min.

The dehydration reaction started at room temperature for all heating rates. The final temperature varied depending on the heating rate, but averaged 108 °C. The mass loss in this process averaged 6.18%. The DSC diagram shows that the process was endothermic (Figure 1c).

Following the completion of the dehydration step, the coal retains its thermal stability up to approximately 225 °C without suffering any noticeable mass loss. The overall

combustion process initiates at around 225 °C and terminates at an average temperature of 604 °C, resulting in a total mass loss of 46.27%. The average enthalpy of combustion calculated from the DSC peak areas for the overall combustion process is 8251.56 ± 117.96 J/g. This value is slightly lower than the enthalpy value determined via the bomb calorimeter (9899.34 ± 120.25 J/g). This minor discrepancy is attributed to the inherent differences in the operating principles and experimental methodologies of the two techniques. Specifically, while the bomb calorimeter involves near-instantaneous combustion accompanied by rapid heating and cooling under sealed, oxygen-rich conditions, the DSC method subjects the sample to a relatively slower, highly controlled thermal regime governed by pre-programmed heating rates. A detailed examination of the TGA curve reveals that this combustion occurs with two distinct slopes (Figure 1a), where the first corresponds to major mass loss, whereas the second reflects a minor mass loss. This two-stage behavior is further supported by the DTG curve, which exhibits two consecutive peaks: a primary peak with a larger peak area associated with the major weight loss and a secondary peak with a smaller area representing a lower percentage of mass consumption (Figure 1b). Furthermore, the DSC profile shows two main exothermic regions. The first exothermic region spans a broader temperature range and features a minor shoulder at its onset, while the second exothermic region covers a narrower interval and is characterized by a sharp peak (Figure 1c). Collectively, these thermal findings demonstrate that combustion does not proceed in a single step, but rather evolves through two consecutive stages defined as "Combustion 1" and "Combustion 2", which were subsequently evaluated through individual kinetic and thermodynamic analyses.

Spanning an average temperature range of 225–496 °C across all heating rates, Combustion 1 accounts for a mass loss of approximately 39%, representing roughly 85% of the overall combustion process. At the onset of Combustion 1, a subtle mass increase is detectable on the TG curve (Figure 1a), accompanied by a corresponding minor exothermic shoulder in the DSC profile (Figure 1c). This transient phenomenon stems from the adsorption of the supplied oxygen onto the coal surface, which occurs simultaneously with the onset of combustion. Because this oxygen adsorption is very limited in scope and quickly dominated by the primary combustion process, it manifests only as a brief, minor mass gain and a subtle thermal shoulder immediately before the main combustion regime. A similar phenomenon was reported by Naktiyok during the study of the oxidation behavior of Tavşanlı coals at low temperatures. The authors noted partial mass increases in the 150–250 °C temperature interval, resulting from the adsorption of oxygen gas by the coal [6]. Furthermore, typical low-rank coal combustion and oxidation studies in the literature confirm that within these specific temperature intervals, the structural changes are predominantly governed by mass loss/gain profiles without any major anomalous chemical transitions [26,27]. This further supports that the experimental thermal pathways captured by our TGA and DSC profiles reflect the genuine, fundamental steps of the Çayırhan coal combustion process.

Depending on the heating rate, Combustion 2 occurs in the average temperature range of 496–604 °C, causing a mass loss of 7.11%. This corresponds to approximately 15% of the overall mass loss during the entire combustion process.

The thermal data obtained at all heating rates for both Combustion 1 and Combustion 2 reactions are summarized in Table 2.

It is not surprising that the onset, end, and peak temperatures shift to higher values as the heating rate increases in both exothermic reactions. This is because a higher heating rate leads to a slight thermal lag in the sample, causing these temperature points to appear at higher values [28].

Table 2. Thermal parameters of Combustion 1 and Combustion 2 stages for Çayırhan coal at different heating rates (values represent ± standard deviation).

Thermal Property	Combustion 1				Combustion 2			
	5	10	15	Average	5	10	15	Average
T_{inital} (°C)	221.61	224.23	227.85	224.56 ± 3.12	489.30	494.17	503.18	495.55 ± 7.04
T_{final} (°C)	489.30	494.17	503.18	495.55 ± 7.04	596.85	605.9	608.63	603.79 ± 6.35
T_{peak} (°C)	383.32	394.63	399.05	392.33 ± 8.12	539.95	549.77	559.59	549.77 ± 9.82
Δm (%)	38.85	38.64	40.00	39.16 ± 0.74	6.27	6.92	8.14	7.11 ± 0.95

For Çayırhan coal, the mineral decomposition reaction begins immediately after combustion. The reaction temperature range is approximately 630–745 °C. The mass loss at the three heating rates for this endothermic reaction averages 6.66%.

3.3. Kinetic and Thermodynamic Analysis for Combustion Reactions of Çayırhan Coal

In this section, the combustion region, which was identified in the thermal analysis section, is examined in detail. Preliminary thermal analysis data (TGA slope alterations, consecutive DTG peaks, and DSC exothermic profiles) suggested that the combustion process might not proceed via a single step but could involve a two-stage mechanism consisting of a faster major mass loss (Combustion 1) followed by a slower minor mass loss (Combustion 2). To validate this behavior and precisely determine the transition between these stages, the entire combustion region was initially evaluated as a single reaction step. The objective here was to monitor the distribution of activation energy and to confirm the validity of splitting the combustion region based on any sharp increase or decrease observed in the E_a values. This approach—evaluating the overall region kinetics to identify sharp fluctuations in activation energy and thereby justify the separation of consecutive reaction steps—was successfully implemented in our previous study on the thermal decomposition kinetics of uranium salts [11–13]. For this combined region, E_a values for different conversion fractions (α) were calculated using the FWO and KAS methods. The graph showing the variation of E_a with α is presented in Figure 2a. An examination of Figure 2a confirms that dividing the combustion region into two distinct stages yields greater consistency. Specifically, up to a conversion fraction of α = 0.80, the activation energy values remain fairly close to one another, ranging between an average of 110 kJ/mol and 130 kJ/mol. However, beyond α = 0.80, a substantial increase in activation energy values is observed. This reveals that treating the entire combustion step as a single reaction would be inappropriate from kinetic and thermodynamic perspectives, and that dividing the process into two stages aligns well with the thermal analysis data. As outlined above, this separation is explicitly corroborated by two independent criteria: thermal-analysis profile features (TG, DTG, and DSC) and model-free kinetic behavior. As depicted in Figure 1a–c, the boundary between Combustion 1 and Combustion 2 is marked by the distinct inflection/valley point following the primary Combustion 1 peak (T_{peak} = 394.63 °C). This thermal boundary precisely coincides with the kinetic transition observed in the KAS and FWO E_a profiles, where α relatively stable activation energy plateau ($\alpha \leq 0.80$) ends and a sharp upward trend begins. The subsequent peak in DTG and DSC (T_{peak} = 549.77 –553.44 °C) corresponds to the char combustion stage, confirming that the thermal and kinetic criteria independently converge to reflect consistent boundaries for this reaction stage.

Using the initial and final temperature values given in Table 2, the combustion process was divided into two stages, and kinetic analysis was performed again for each stage. As seen in Figure 2b, in Combustion 1, E_a values increase gradually up to a combustion ratio of α = 0.60. Then, a decrease in E_a values is observed up to α = 0.80. After α = 0.80, E_a values

begin to increase again. The increase in this region may be considered as preparation for Combustion 2. The E_a values calculated using the KAS and FWO methods are consistent with each other. Average E_a values are 137.92 ± 9.75 and 141.38 ± 9.52 kJ/mol, respectively. The high reliability of the calculation is further supported by the regression analysis results, which yielded values of 0.997 ± 0.004 and 0.998 ± 0.003, respectively.

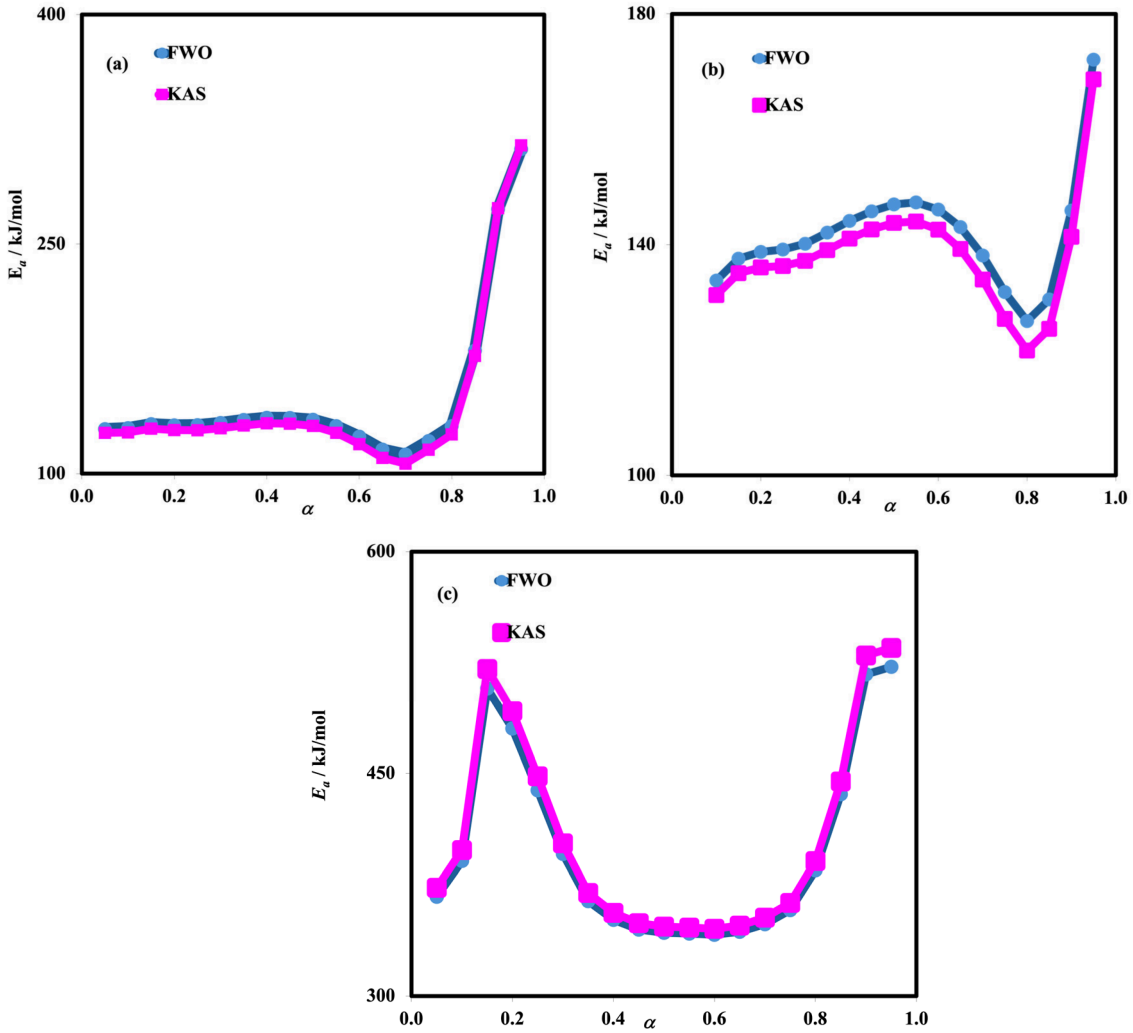


Figure 2. Variation of activation energy (E_a) with respect to conversion fraction (α): (**a**) combined overall combustion region, (**b**) Combustion 1 stage, and (**c**) Combustion 2 stage.

An examination of Figure 2c reveals that the E_a values for Combustion 2 are considerably higher and fluctuate over a broad range, varying between 340 and 540 kJ/mol. In this region, the activation energy exhibits a notable increase at both low (α = 0.20) and high conversion fractions (α = 0.85 and 0.90). One possible explanation for this increase is that mass and heat transfer limitations could potentially occur, affecting the diffusion of evolved gases or oxygen transport during these specific combustion ratios. The average E_a values calculated using the KAS and FWO methods are 405.82 ± 67.96 and 398.72 ± 64.67 kJ/mol, respectively.

When evaluating the overall progressive changes in activation energies across both zones, several important characteristics stand out in comparison with the literature. To the best of our knowledge, while no previous study has investigated the combustion kinetics of Çayırhan coal with such high compositional resolution, the observed E_a trends align well with the general combustion profiles of other low-rank coals. The upward trend in E_a values starting at the end of Combustion 1 (α = 0.80) represents the transition from the rapid

stage to the char combustion stage, where the remaining structurally stable carbonaceous matrix requires higher energy input to undergo oxidation. Furthermore, the notably high E_a values (340–540 kJ/mol) and the significant fluctuations observed during the final stages of Combustion 2 (α = 0.85 and 0.90) are highly consistent with literature reports on coal combustion. This phenomenon is typically attributed to severe mass and heat transfer limitations; as combustion progresses, the accumulation of ash layers around the unburnt char core creates a strong structural barrier that severely hinders oxygen transport and gas diffusion [7,8,29,30].

Table 3 presents the E_a values, which were calculated using the KAS and FWO methods for different conversion fractions of Combustion 1 and Combustion 2, along with the regression analysis values. High regression analysis values indicate high linearity in the calculations. The initial stage of combustion requires low activation energy, rendering it a kinetically favorable process with a lower energy barrier. Conversely, the second combustion stage—representing 15% of the total reaction—requires a remarkably high activation energy to proceed, reflecting lower reactivity and a higher kinetic barrier relative to the energy release stage.

Table 3. Calculated activation energies (E_a) and determination coefficients (r^2) for Combustion 1 and Combustion 2 stages using KAS and FWO methods across progressive conversion fractions (α).

Reac.	**Combustion 1**				**Combustion 2**			
Method	**KAS**		**FWO**		**KAS**		**FWO**	
α	E_a	r^2	E_a	r^2	E_a	r^2	E_a	r^2
0.05	134.14	0.999	136.21	0.999	373.00	0.944	366.89	0.948
0.10	131.27	1.000	133.78	1.000	398.28	0.972	391.03	0.974
0.15	135.04	0.999	137.58	0.999	520.66	0.913	507.52	0.917
0.20	136.07	1.000	138.74	1.000	491.91	0.947	480.27	0.950
0.25	136.31	1.000	139.15	1.000	448.12	0.972	438.72	0.974
0.30	137.21	1.000	140.17	1.000	402.86	0.985	395.75	0.986
0.35	139.07	1.000	142.10	1.000	369.43	0.993	364.03	0.994
0.40	141.04	0.999	144.12	1.000	355.97	0.998	351.28	0.999
0.45	142.65	0.999	145.78	0.999	349.09	1.000	344.78	1.000
0.50	143.78	0.998	146.99	0.998	346.71	1.000	342.55	1.000
0.55	144.01	0.997	147.33	0.998	346.11	1.000	342.02	1.000
0.60	142.59	0.996	146.10	0.996	345.23	1.000	341.21	1.000
0.65	139.25	0.994	143.05	0.995	347.42	1.000	343.33	1.000
0.70	133.94	0.991	138.13	0.993	352.76	1.000	348.44	1.000
0.75	127.12	0.989	131.79	0.991	362.72	0.998	357.95	0.998
0.80	121.64	0.990	126.75	0.992	390.85	0.999	384.75	0.999
0.85	125.41	0.995	130.51	0.996	444.65	1.000	435.98	1.000
0.90	141.38	0.999	145.89	0.999	529.85	0.998	517.11	0.998
0.95	168.65	0.999	172.07	0.999	534.88	0.994	522.08	0.994
Mean	137.92	0.997	141.38	0.997	405.82	0.985	398.72	0.986

Subsequent to model-free kinetic analysis, efforts were concentrated on identifying the appropriate combustion kinetic model by testing 13 different model equations. When determining the most suitable model equation, the following factors are considered together: (i) The closeness of the activation energy value determined by each model to the average activation energy value calculated using model-free methods (using the KAS equation for CM I and the FWO equation for CM II) is evaluated. (ii) High regression analysis values of the resulting graphs are evaluated. (iii) If different heating rates have been examined, it is assessed whether the activation energy values in the selected model are close to each other (low standard deviation) for each of these heating rates.

For Combustion 1, the graphs plotted using the CM I and CM II methods at each heating rate indicated that the D_3 model provided the best kinetic description among the tested model functions. Under this model framework, mass transfer limitations—such as resistance in gaseous product release or reactive gas transport—are considered as potential contributing factors influencing the kinetic reaction behavior. The relevant graphs are given in Figure 3a,b. The other thermodynamic parameters were calculated from best-fit model equations and were tabulated in Table 4.

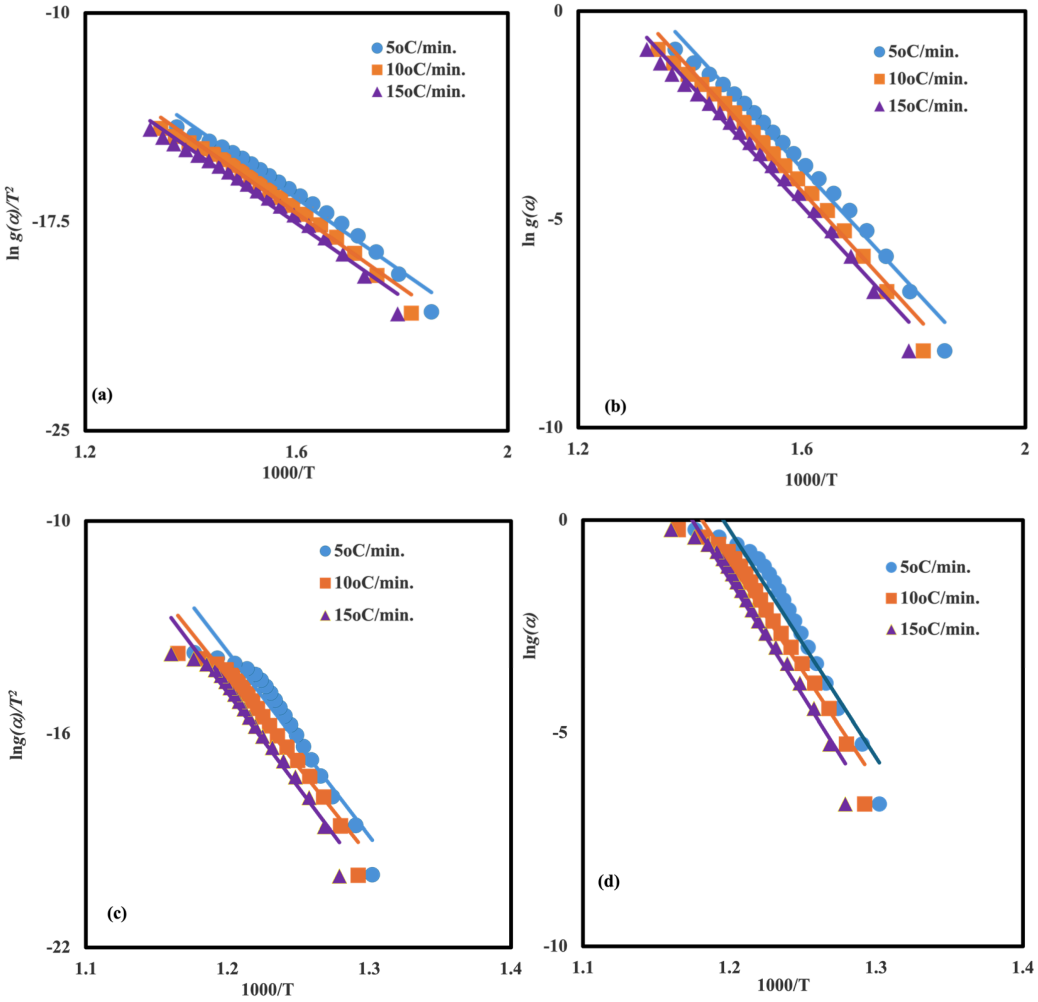


Figure 3. Kinetic fitting graphs based on Composite Methods: (**a**) Combustion 1 using CM I, (**b**) Combustion 1 using CM II, (**c**) Combustion 2 using CM I, and (**d**) Combustion 2 using CM II.

Table 4. Kinetic and thermodynamic parameters calculated for the Combustion 1 stage using CM I and CM II methods at different heating rates.

Method	**CM I**				**CM II**			
β (°C/min)	5	10	15	Mean	5	10	15	Mean
r^2	0.98	0.98	0.98	0.98	0.98	0.98	0.98	0.98
E_a (kJ/mol)	109.91	111.47	110.29	110.56	114.38	110.84	115.14	113.45
ln A	15.70	16.16	15.98	15.94	17.13	16.33	16.79	16.75
$\Delta H^{\ddagger}$ (kJ/mol)	104.63	106.08	104.81	105.17	109.10	105.44	109.65	108.06
$\Delta S^{\ddagger}$ (J/mol.K)	−120.68	−117.02	−118.69	−118.80	−109.06	−115.60	−111.60	−112.08
$\Delta G^{\ddagger}$ (kJ/mol)	181.26	182.04	183.09	182.13	178.34	180.48	183.26	180.69

To statistically evaluate the applicability of the D_3 model for Combustion 1, other candidate mechanisms were systematically examined. For instance, the nucleation-based model (A_3) yielded an overall average r^2 of 0.93 and an average E_a of 21.22 kJ/mol. The phase-boundary model (R_2) displayed an average r^2 of 0.90 with an average E_a of 53.55 kJ/mol, while the standard reaction order-based model (F_2) exhibited an average r^2 of 0.81 and an average E_a of 42.61 kJ/mol. These alternative functions exhibited lower correlation and higher kinetic deviations from the model-free parameters, suggesting they are less representative of the process.

In sharp contrast, the selected D_3 model demonstrated exceptional statistical and kinetic reliability, maintaining an avg. r^2 of 0.98 across both composite frameworks. Furthermore, the combined average activation energy derived from CM I and CM II for the D_3 model was calculated as 112.00 kJ/mol. This composite value shows a reasonable physical consistency with the average E_a profiles independently obtained from the model-free methods (139.65 $\pm$ 9.66), with a relative deviation of approximately 19.8%. Considering the fundamental mathematical differences between model-fitting (which assumes a single reaction mechanism) and model-free kinetics (which accounts for local conversion-dependent variations), this alignment indicates that the D_3 model serves as a reasonable kinetic representation for describing the Combustion 1 stage.

Modeling studies were also conducted for Combustion 2, where a diffusion-controlled mechanism was similarly found to be dominant. Specifically, the D_2 model provided the optimal kinetic fit for this stage. The variation in E_a profiles observed in the model-free analysis aligns with a shift in the apparent diffusion kinetics. The kinetic curves obtained using this model are shown in Figure 3c,d, while the calculated thermodynamic parameters of the activated complex are summarized in Table 5.

Table 5. Kinetic and thermodynamic parameters calculated for the Combustion 1 stage using CM I and CM II methods at different heating rates.

Method	**CM I**				**CM II**			
β (°C/min)	5	10	15	Mean	5	10	15	Mean
r^2	0.97	0.96	0.97	0.97	0.96	0.97	0.98	0.97
E_a (kJ/mol)	431.74	416.92	442.22	430.29	423.23	409.25	433.40	421.96
ln A	61.13	58.91	62.60	60.88	60.12	57.99	61.57	59.89
$\Delta H^{\ddagger}$ (kJ/mol)	425.02	410.13	435.38	423.51	416.51	402.46	426.56	415.18
$\Delta S^{\ddagger}$ (J/mol.K)	267.10	236.51	255.03	252.88	246.64	228.80	258.56	244.67
$\Delta G^{\ddagger}$ (kJ/mol)	209.05	216.91	225.46	217.14	217.10	215.53	213.74	215.45

A similar screening protocol based on the combined averages of CM I and CM II was executed for Combustion 2 to evaluate the statistical performance of the D_2 model. For instance, the nucleation-based model (A_3) yielded an overall average r^2 of 0.92 and an average E_a of 86.22 kJ/mol. The phase-boundary model (R_2) displayed an avg. r^2 of 0.91 with an average E_a of 226.12 kJ/mol, while the standard reaction order-based model (F_2) exhibited an average r^2 of 0.85 and an average E_a of 184.14 kJ/mol. These alternative functions were deemed less suitable due to their lower regression linearity and higher deviations from model-free estimations.

In sharp contrast, the selected D_2 model demonstrated exceptional statistical and kinetic reliability, maintaining an average r^2 of 0.97 across both composite frameworks. Furthermore, the combined average activation energy derived from CM I and CM II for the D_2 model was calculated as 426.12 kJ/mol. This composite value shows a high

physical consistency with the average E_a profiles derived from the model-free methods (402.27 ± 65.53 kJ/mol), exhibiting a minor relative deviation of approximately 5.9%. This close numerical alignment suggests that the D_2 model effectively describes the kinetic behavior of the Combustion 2 stage.

While high r^2 values indicate strong statistical correlation, the suitability of the selected kinetic functions was further supported through Master Plot analysis (CM I and CM II).

In diffusion-controlled processes, structural accumulation during reaction progress enhances mass transfer resistance, leading to a continuous increase in activation energy. Diffusion limitations, which initiate during Combustion 1, become significantly more pronounced during the Combustion 2 stage. This kinetic evolution reflects a transitional shift from the early chemical/reaction activity stage governed by volatile release toward a highly constrained diffusion regime during char oxidation. This situation is also explained in the academic literature. Çılgı and Ak formed a copolymer by reacting the N-(4-(3-Thienyl methylene)-oxycarbonylphenyl) maleimide monomer they synthesized with styrene and investigated the thermal decomposition kinetics of the resulting molecule. In the study, the activation energy showed a continuous upward trend. In the modeling study conducted for thermodynamic investigation purposes, it was found that the reaction was consistent with the D_1 diffusion model [31]. Furthermore, Li and colleagues stated that the three-dimensional diffusion model (D_3) is effective in the combustion kinetics of coal from the Chinese region [15], which strongly supports our findings. The accumulated ash boundary layers and structural char shrinkage during the progressive stages of Çayırhan coal combustion systematically intensify the mass transfer resistance, thereby requiring higher activation energy values fully consistent with literature models.

$\Delta S^{\ddagger}$ represents the disorder of the system. Negative $\Delta S^{\ddagger}$ values indicate that the activated complex has lower rotational and vibrational freedoms. Furthermore, positive $\Delta G^{\ddagger}$ values indicate that combustion did not occur spontaneously and that heat input is a precursor to the reaction. The results are consistent with the academic literature [15,32].

4. Conclusions

The multi-step thermal degradation, kinetic evolution, and thermodynamic behavior of Çayırhan coal during combustion were comprehensively evaluated using model-independent (KAS and FWO) and model-fitting (CM I and CM II) approaches. The main conclusions drawn from this investigation are summarized as follows:

- ✓ The combustion process proceeds sequentially through two distinct thermal stages rather than a single-step reaction, with Combustion 1 accounting for approximately 85% of the total thermal degradation.
- ✓ Kinetic modeling suggests a transition in the apparent rate-controlling behavior, where the experimental data are best described by a 3D diffusion model in the initial stage and shift toward a 2D diffusion model in the final stage, likely driven by mass and heat transfer limitations within the coal matrix.
- ✓ From an energy perspective, fostering combustion primarily within Combustion 1 may offer operational advantages by promoting favorable reaction kinetics and reducing the activation energy input required to sustain the process.

Overall, while these laboratory-scale findings offer functional insights for coal-based energy recovery processes, they should be interpreted as foundational guidelines rather than direct scaling values for industrial reactor design.

Author Contributions: G.K.Ç.: Investigation, Conceptualization, Methodology, Writing—review and editing, Project administration. E.Ç.: Investigation, Formal analysis, Validation. All authors have read and agreed to the published version of the manuscript.

Funding: This research was funded by the Scientific Research Projects Unit of Manisa Celal Bayar University, grant number BAP 2024-129.

Data Availability Statement: All data generated or analyzed during this study are included in this published article. Furthermore, any additional raw data or specific datasets can be obtained from the corresponding author upon reasonable request.

Acknowledgments: During the preparation of this manuscript, the authors used Gemini 1.5 Flash (Google) for the purposes of English language editing, proofreading, and improving overall clarity. The authors have reviewed and edited the output and take full responsibility for the content of this publication.

Conflicts of Interest: The author declares no conflicts of interest.

Abbreviations

The following abbreviations are used in this manuscript:

TGA	Thermogravimetric Analysis
DTG	Differential Thermogravimetry
DSC	Differential Scanning Calorimetry
FWO	Flynn–Wall–Ozawa
KAS	Kissinger–Akahira–Sunose
CM I	Composite Method I
CM II	Composite Method II
GCV	Gross Calorific Value
NCV	Net Calorific Value

References

1. Köse, E.; Kutlu Kaynar, S. Energy demand forecasting and policy development in Turkey. *Energies* **2025**, *18*, 3301. [CrossRef]
2. Naktiyok, J.; Özer, A.K. Investigation of combustion process of different coal by TGA Analysis. *KSU J. Eng. Sci.* **2022**, *25*, 691–701.
3. Magalhães, D.; Kazanç, F.; Riaza, J.; Erensoy, S.; Kabaklı, Ö.; Chalmers, H. Combustion of Turkish lignites and olive residue: Experiments and kinetic modelling. *Fuel* **2017**, *203*, 868–876. [CrossRef]
4. Wang, H.; Du, W.; Xi, Y.; Zhang, Y.; Wang, B.; Sun, Y. Non-isothermal thermogravimetric analysis study on the pyrolysis reaction kinetics of bituminous coal. *Chem. Eng. Technol.* **2022**, *45*, 1048–1057. [CrossRef]
5. Zhang, Y.; Zhang, Y.; Li, Y.; Shi, X.; Che, B. Determination of ignition temperature and kinetics and thermodynamics analysis of high-volatile coal based on differential derivative thermogravimetry. *Energy* **2022**, *240*, 122493. [CrossRef]
6. Naktiyok, J. Investigation of the oxidation behavior of a Turkey coal at low temperature by TGA, FTIR and BET analysis. *Energy Sources Part A* **2020**, *42*, 2370–2380. [CrossRef]
7. Dwivedi, K.K.; Shrivastav, P.; Karmakar, M.K.; Pramanick, A.K.; Chatterjee, P.K. A comparative study on pyrolysis characteristics of bituminous coal and low-rank coal using thermogravimetric analysis (TGA). *Int. J. Coal Prep. Util.* **2022**, *42*, 1–11. [CrossRef]
8. Yan, J.; Yang, Q.; Zhang, L.; Lei, Z.; Li, Z.; Wang, Z.; Ren, S.; Kang, S.; Shu, H. Investigation of kinetic and thermodynamic parameters of coal pyrolysis with model-free fitting methods. *Carbon Resour. Convers.* **2020**, *3*, 173–181. [CrossRef]
9. Fan, H.; Wang, K.; Zhai, X.; Hu, L. Combustion Kinetics and Mechanism of Pre-Oxidized Coal with Different Oxygen Concentrations. *ACS Omega* **2021**, *6*, 19170–19182. [CrossRef] [PubMed]
10. Kök, M.V.; Özbas, E.; Hicyılmaz, C.; Karacan, Ö. Effect of particle size on the thermal and combustion properties of coal. *Thermochim. Acta* **1997**, *302*, 125–130. [CrossRef]
11. Cetişli, H.; Koyundereli Çılgı, G.; Donat, R. Thermal and kinetic analysis of uranium salts Part 1. Uranium (VI) oxalate hydrates. *J. Therm. Anal. Calorim.* **2012**, *108*, 1213–1222. [CrossRef]
12. Koyundereli Çılgı, G.; Cetişli, H.; Donat, R. Thermal and kinetic analysis of uranium salts Part 2. Uranium (VI) acetate hydrates. *J. Therm. Anal. Calorim.* **2012**, *110*, 127–135. [CrossRef]
13. Koyundereli Çılgı, G.; Cetişli, H.; Donat, R. Thermal and kinetic analysis of uranium salts: Part III. Uranium (IV) oxalate hydrates. *J. Therm. Anal. Calorim.* **2014**, *115*, 2007–2020. [CrossRef]
14. *ASTM D5373*; Standard Test Methods for Instrumental Determination of Carbon, Hydrogen, and Nitrogen in Laboratory Samples of Coal and Coke. ASTM International: West Conshohocken, PA, USA, 2021.
15. Li, Q.; Xiao, Y.; Wang, C.; Deng, J.; Shu, C. Thermokinetic characteristics of coal spontaneous combustion based on thermogravimetric analysis. *Fuel* **2019**, *250*, 235–244. [CrossRef]

16. Conesa, J.A. Numerical integration of weight loss curves for kinetic analysis. *Thermo* **2021**, *1*, 32–44. [CrossRef]
17. Ak, M.; Koyundereli Çılgı, G.; Kuru, F.D.; Cetişli, H. Thermal decomposition kinetics of polypyrrole and its star-shaped copolymer. *J. Therm. Anal. Calorim.* **2013**, *111*, 1627–1632. [CrossRef]
18. Söyleyici, S.; Koyundereli Çılgı, G. Thermal and kinetic analyses of 2,5-bis(2-hydroxyphenyl)thiazolo [5,4-d]thiazole. *J. Therm. Anal. Calorim.* **2014**, *118*, 705–709. [CrossRef]
19. Jayaraman, K.; Kök, M.V.; Gökalp, İ. Combustion mechanism and model-free kinetics of different origin coal samples: Thermal analysis approach. *Energy* **2020**, *204*, 117905. [CrossRef]
20. Budrugeac, P.; Segal, E. On the use of Diefallah's composite integral method for the non-isothermal kinetic analysis of heterogeneous solid-gas reactions. *J. Therm. Anal. Calorim.* **2005**, *82*, 677–680. [CrossRef]
21. Koyundereli Çılgı, G. Effect of atmospheric condition on the thermal decomposition kinetics and thermodynamics of lead acetate trihydrate. *Indian J. Chem. Technol.* **2023**, *30*, 560. [CrossRef]
22. Gabal, M.A. Non-isothermal studies for the decomposition course of CdC_2O_4–ZnC_2O_4 mixture in air. *Thermochim. Acta* **2004**, *412*, 55–62. [CrossRef]
23. Wendlant, W.W. *Thermal Analysis*, 3rd ed.; John Wiley: New York, NY, USA, 1986.
24. Yang, Y.; Li, J. Investigation of macro-kinetics of coal-oxygen reactions under varying oxygen concentrations: Towards the understanding of combustion characteristics in underground coal fires. *Process Saf. Environ. Prot.* **2022**, *160*, 232–241. [CrossRef]
25. Janković, B.; Manić, N.; Radović, I.; Janković, M.; Rajačić, M. Model-free and model-based kinetics of the combustion process of low rank with high ash contents using TGA-DTG-stage-MS and FTIR techniques. *Thermochim. Acta* **2019**, *679*, 178337. [CrossRef]
26. Wei, S.; Wei, Y.; Li, Z. Influence of different particle sizes on spontaneous combustion characteristics of coal. *Solid Fuel Chem.* **2025**, *59*, 48–52. [CrossRef]
27. Hu, L.; Wang, K.; Deng, J.; Yu, Y.; Zhang, Y.; He, J. Thermodynamics of coal oxidation mass gain behavior based on parallel reaction model by TG and DSC. *J. Therm. Anal. Calorim.* **2024**, *149*, 14741–14751. [CrossRef]
28. Aboni Akodzi, M.C.; Girods, P.; Andzi-Barhé, T.; Rogaume, Y. Study of the pyrolysis of ayous and kambala co-products: Kinetic modeling of the two species. *Thermo* **2024**, *4*, 490–507. [CrossRef]
29. Sis, H. Application of model-free methods for analysis of combustion kinetics of coals with different ranks. *Energy Sources Part A Recovery Util. Environ. Eff.* **2009**, *31*, 1016–1027. [CrossRef]
30. Zhang, Y.; Guo, Y.; Cheng, F.; Yan, K.; Cao, Y. Investigation of combustion characteristics and kinetics of coal gangue with different feedstock properties by thermogravimetric analysis. *Thermochim. Acta.* **2015**, *614*, 137–148. [CrossRef]
31. Koyundereli Çılgı, G.; Ak, M. Thermal degradation kinetics and thermodynamics of maleimide-sytrene based alternating copolymer: A comparative investigation of monomer and polymer structures. *J. Mol. Struct.* **2020**, *221*, 128879. [CrossRef]
32. Gao, M.; Cheng, C.; Miao, Z.; Wan, K.; He, Q. Physicochemical properties, combustion kinetics and thermodynamics of oxidized lignite. *Energy* **2023**, *268*, 12665. [CrossRef]

Disclaimer/Publisher's Note: The statements, opinions and data contained in all publications are solely those of the individual author(s) and contributor(s) and not of MDPI and/or the editor(s). MDPI and/or the editor(s) disclaim responsibility for any injury to people or property resulting from any ideas, methods, instructions or products referred to in the content.